Proceedings of the
Annual Stability Conference
Structural Stability Research Council
Louisville, Kentucky, April 1-4, 2025

Experiments to understand the impact of local and global slenderness on inelastic deformation capacity of round HSS braces

Lily A. Swanson[1], Dawn E. Lehman[2], Jeffrey W. Berman[3], Charles W. Roader[4], Andrew D. Sen[5]

Abstract
This paper presents preliminary results from an experimental research program conducted at the University of Washington on the inelastic deformation capacity of round HSS braces. This research aimed to identify the relationship between local and global slenderness on the drift capacity of braces used in ordinary and special concentrically braced frames to evaluate the AISC 342-22 moderately and highly ductile limits. The study used a specimen test matrix that included a wide range of local slenderness (i.e., diameter-to-thickness) and global slenderness ratios of round HSS. The range of local slenderness ratios encompassed those meeting and not meeting the high and moderate ductility limits in the AISC Seismic Provisions. The test results demonstrate that the moderate and high ductility limits in AISC 341-22 for round HSS are overly conservative. Furthermore, it was observed that global slenderness significantly impacts brace ductility in that increasing a brace's global slenderness can sustain higher local slenderness while still meeting deformation capacity targets. This suggests that the local slenderness limits would give a more accurate definition of ductility if written as a function of both local and global slenderness.

1. Introduction

HSS braces are designed to be the fuse element in concentrically braced frame (CBF) systems through inelastic yielding in tension and buckling in compression. Large axial deformations lead to the formation of a plastic hinge at the midspan of the brace. Also referred to as cupping, the plastic hinge forms and develops large strains due to local deformations. Local deformations seen in Figure 1 show the progression of deformation starting at the initiation of visible cupping. Cupping is the onset of damage that indicates that the brace is now susceptible to tearing and fracturing in tension. Tearing of the cupping region begins at the top and bottom corners of the brace in tension after cupping. Fracture occurs almost immediately after tearing. A favorable brace has the ability to withstand large axial deformations before the formation of cupping at the plastic hinge.

[1] Graduate Research Assistant, University of Washington, <swanlily@uw.edu>
[2] Professor, University of Washington, <delehman@uw.edu>
[3] Professor, University of Washington, <jwberman@uw.edu>
[4] Professor Emeritus, University of Washington, <croeder@uw.edu>
[5] Professor, Marquette University, <andrew.sen@marquette.edu>

Figure 1: Progression of Damage at Brace Midspan

In comparison to square HSS braces, the testing of circular HSS braces is much more limited; There are few tests on circular sections made from modern steels, such as A500C and A1085. Further testing is required to assess and possibly revise the current local slenderness limits. The following summarizes two studies on the cyclic testing of round HSS braces.

Elchalakani et al. (2003) tested a series of cold-formed round circular tube braces made from AS1163 (1991) Grade C350L0 steel, an Australian designation. Their test program used sections with width-to-thickness ratios from 32 to 55 and global slenderness between 30 and 55. The results of the tests show that the specimen's ductility capacity ratio (the ratio of peak deformation to yield deformation) was between 1.4 and 2.7 prior to brace fracture and that fracture life depends heavily on the occurrence of local cupping.

Takeuchi and Masui (2011) conducted tests on circular tube braces made from STK400, Japanese steel. The specimens had width-to-thickness ratios between 21 and 32 and global slenderness ratios ranging from 53 to 121. The strain concentration ratio (the ratio between the hinge region strain and the average strain along the brace) significantly increased as brace local slenderness increased and global slenderness decreased.

Two geometric properties are known to affect brace performance and deformability: brace global slenderness, L_c/r, and local slenderness, D/t. L_c is the effective brace length, r is the radius of gyration, D is the outside diameter, and t is the wall thickness. The current AISC equations limiting diameter-to-thickness ratios for moderate and highly ductile HSS braces from AISC Table D1.1a are summarized:

$$\lambda_{md} = 0.062\frac{E}{R_y F_y} \tag{1}$$

$$\lambda_{hd} = 0.053\frac{E}{R_y F_y} \tag{2}$$

The moderately ductile limit, Eq. 1, provides the maximum diameter-to-thickness ratio for ordinary concentrically braced frames (OCBFs) and the highly ductile limit, Eq. 2, provides the maximum diameter-to-thickness ratio for special concentrically braced frames (SCBFs). The current limits are not dependent on global slenderness. They are only dependent on the modulus of elasticity, E, the ratio of the expected yield stress to the specified minimum yield stress, R_y, and the nominal yield stress, F_y. All braces in this study were made of A500 Gr. C steel. The material specifications and corresponding moderately and highly ductile limits can be found in Table 1.

Table 1: HSS Specifications and Provisions for A500 Gr. C Steel

Property	ASTM A500 Gr. C
Yield Strength Ratio, Ry	1.3
Yield Stress	50 ksi (min)
Tensile Stress	62 ksi (min)
Moderately Ductile Limit, λ_{md}	27.7
Highly Ductile Limit, λ_{hd}	23.6

Recent research at the University of Washington Structural Research Laboratory (UW SRL) investigated the response of A1085 and A500 square HSS braces conducted by Bergendahl, 2021 and Kaldestad, 2022 (denoted *Previous Research* herein). The test setup utilized in this study was designed and first used in that previous research. Bergendahl, 2021 and Kaldestad, 2022 tested braces with local slenderness ranging from 9 to 25.7 and global slenderness ranging from 60 to 127. Minimal data exists on the brace performance of round HSS using modern steel which motivated the research performed in this study. Twenty-one round A500 HSS braces of various local and global slenderness were tested in this research program.

2. Testing Program and Specimen Design

This section provides an overview of the test setup, specimen design, test matrix, and loading protocol. The testing rig was designed to accommodate HSS specimens of varying cross-section sizes and lengths. A displacement controlled symmetric loading protocol was applied using the testing rig that was suited to move axial displacements of ±10 inches and could generate brace axial forces of up to 1000 kips in tension and 700 kips in compression. Twenty-one round A500 HSS were tested to evaluate their cyclic performance.

2.1 Test Setup and Specimen Design

The test frame was designed to handle a variety of HSS brace sizes and lengths, allowing for the study of a broad range of local slenderness and global slenderness ratios. In this testing program, two different brace specimen lengths were tested. The test setup in Figure 2, accommodated the 219.5” specimens – the long brace length. An additional 36” deep small reaction block was added to the north side of the end reaction block to shorten the clear distance between the end reaction block and the sliding beam. The test setup with the additional end reaction block, accommodated the 183.5” specimens – the short brace length. Brace lengths were limited by anchor hole locations on the UW SRL strong floor.

Cyclic loads were applied using two hydraulic actuators operating in parallel. The actuators operating in unison could apply a maximum combined brace force of 1000 kips in tension and 700 kips in compression. The capacity of each component in the test setup was designed based on these maximum loads. The south and actuator reaction blocks are fixed to the strong floor while the actuator forces are applied to move the sliding beam. The sliding beam is able to slide on a near-frictionless surface to apply the full actuator force through the connection plates to the specimen.

Test specimens were fabricated at the UW SRL. The test specimens were cut to length using a horizontal band saw and slotted at both ends with a plasma cutter. The cut-to-length specimens were welded to gusset plates which were connected to the reaction block and sliding beam through steel connection plates and twelve 1-inch diameter A490 bolts. To control the direction of out-of-plane buckling, a 3/16” eccentricity was used to offset the center of the brace and the center of the connection. The eccentricity was intended to control the direction of global buckling (towards the East) but not compromise the strength of the member. The test specimen detailed in Figure 3 is the final layout of the long brace length specimen before testing.

Multiple instruments were utilized to collect data on forces, displacements, and strains during testing. The devices used during testing included string potentiometers, duncan potentiometers, strain gauges, load cells, Linear Variable Differential Transformers (LVDTs), and Optotrak sensors. String potentiometers were attached to key locations on specimens to collect data on brace axial deformation, transverse displacement, gusset plate rotation, and bolt slip.

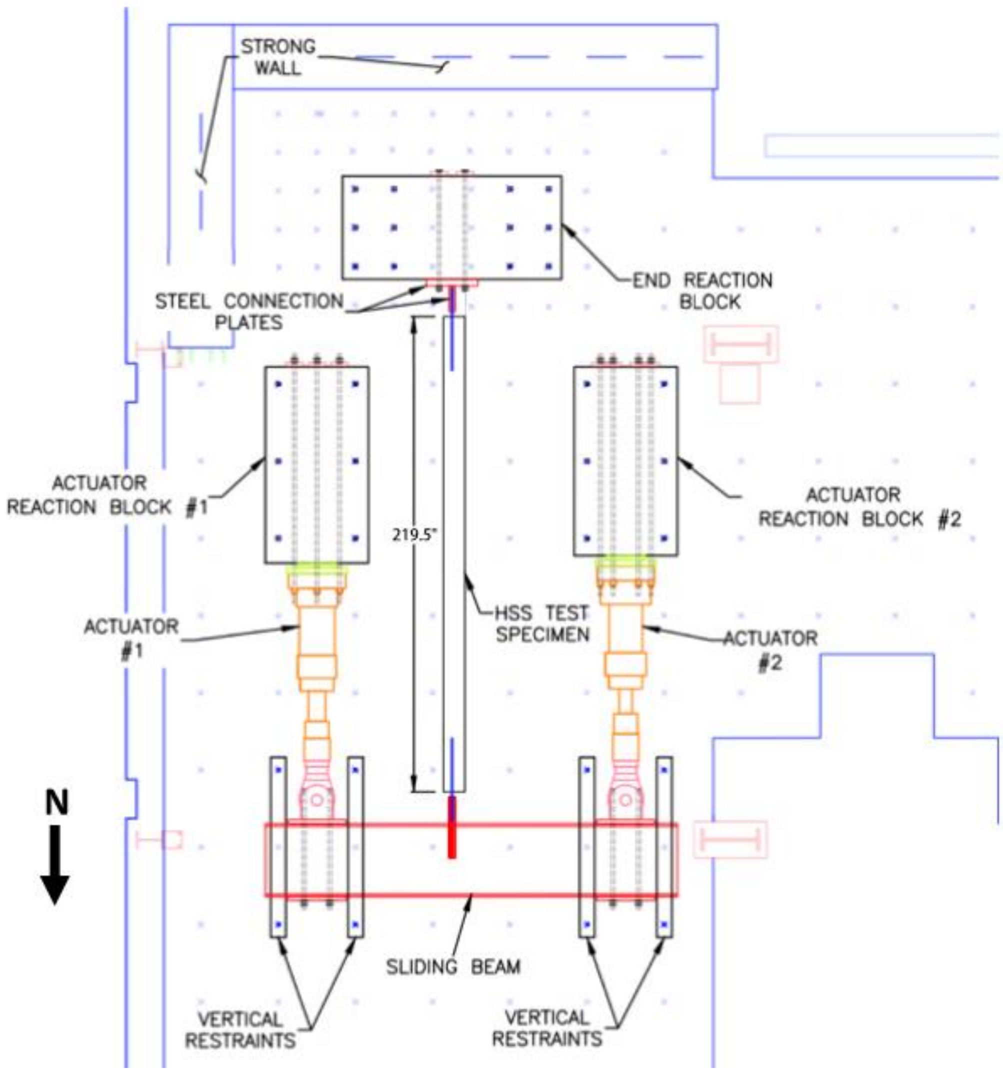

Figure 2: Overview of Test Frame for 219.5” Specimens

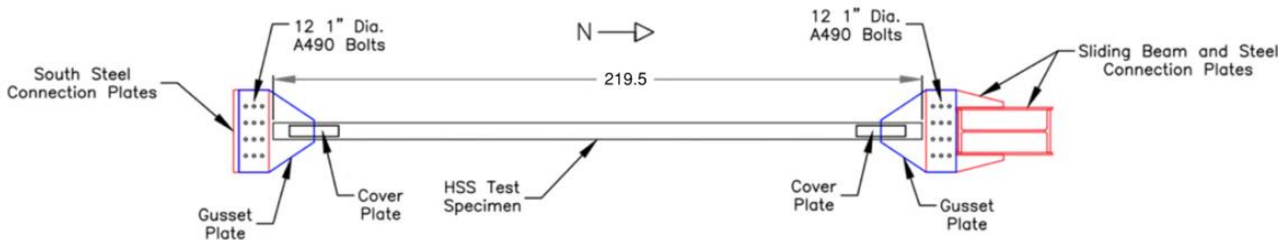

Figure 3: Test Specimen Layout

2.2 Test Matrix

The ductility of a brace is its capacity to withstand inelastic deformations while maintaining sufficient strength and avoiding early fracture. Local slenderness and global slenderness were the basis of how HSS sections were selected in this research to evaluate the current ductility limits in AISC 341-22. Braces were chosen to collect data over a broad range brace local and global slenderness. The nominal diameter-to-thickness ratios of the round specimens are summarized in Table 2. Specimen names ending in an “S” denote that the brace is 183.5” – the short brace length. All other braces are 219.5” long – the long brace length. The nominal diameter-to-thickness ratios in Table 2 are color-coded based on what limits they do or do not satisfy in AISC 341-22 Table D1.1a. Green indicates HSS that meets the criteria for highly ductile braces, orange represents HSS that meets the standards for moderately ductile braces, and red signifies HSS that fails to meet either of the limits specified in The Seismic Provisions – noted in Table 1.

Table 2: Geometric properties of Test Specimens

Specimen	D/t_{no}	D/t_{meas}	$D/t_{meas}/D/t$	L_c/r
HSS6x3/16 S	34.5	30.8	0.89	89.1
HSS6x3/16	34.5	34.1	0.99	106.6
HSS6x1/4 S	25.8	24.5	0.95	90.0
HSS6x1/4	25.8	24.7	0.96	107.6
HSS6.625x3/16	38.1	36.7	0.96	96.3
HSS6.625x1/4 S	28.4	28.0	0.99	81.2
HSS6.625x1/4	28.4	27.4	0.96	97.1
HSS6.625x3/8 S	19.0	18.8	0.99	82.7
HSS6.625x3/8	19.0	19.0	1.00	98.9
HSS6.625x1/2 S	14.2	14.1	0.99	84.2
HSS6.625x1/2	14.2	14.5	1.02	100.7
HSS8.625x3/16 S	49.6	46.1	0.93	61.4
HSS8.625x3/16	49.6	43.4	0.88	73.4
HSS8.625x1/4 S	37.0	37.1	1.00	61.8
HSS8.625x1/4	37.0	35.6	0.96	73.9
HSS8.625x3/8 S	24.7	25.0	1.01	62.6
HSS8.625x3/8	24.7	24.4	0.99	74.9
HSS10.750x1/4 S	46.1	46.4	1.01	49.3
HSS10.750x1/4	46.1	43.2	0.94	59.0
HSS10.750x0.365 S	31.7	31.8	1.00	49.9
HSS10.750x0.365	31.7	30.8	0.97	59.6

Tension tests were performed to compare measured, nominal, and provided mill certification data of brace material. A laser extensometer and YFLA strain gauges were applied to each coupon specimen following methods from ASTM A370-24a to collect data. A 2” gauge length was used for the laser extensometer to calculate percent elongation. Data processed from the coupon tests can be found in Table 3. A nominal value of 50 ksi and 62 ksi were used for yield stress and tensile stress respectively to calculate measured yield and tensile overstrength. For comparison, AISC 341-22 Table A3.2 specifies values of R_y equal to 1.3 and R_t equal to 1.2 for A500 Gr. C steel. The average ratio of all the tested sections is similar to the AISC-specified values the ratio of expected to nominal strength. All the measured yield strengths were at least ten percent higher than the specified nominal value.

Table 3: Summary of Material Testing

HSS Shape	**Measured Yield Strength, $F_{y,m}$ (ksi)**	**Measured Yield Strength Ratio, $R_{y,m}$**	**Measured Tensile Strength, $F_{u,m}$ (ksi)**	**Measured Tensile Strength Ratio, $R_{t,m}$**	**Percent Elongation (%)**
6x3/16	53.6	1.1	73.4	1.2	33.2
6x1/4	54.2	1.1	71.6	1.2	40.5
6.625x3/16	56.5	1.1	76.8	1.2	34.8
6.625x1/4	59.0	1.2	74.6	1.2	36.2
6.625x3/8[1]	58.3	1.2	63.7	1.0	-
6.625x1/2	63.7	1.3	66.0	1.1	36.7
8.625x3/16	69.5	1.4	81.6	1.3	29.5
8.625x1/4	67.0	1.3	79.5	1.3	30.3
8.625x3/8	65.7	1.3	75.2	1.2	36.0
10.750x1/4	62.7	1.3	74.8	1.2	34.2
10.750x0.365	60.4	1.2	77.0	1.2	35.6

1.Percent elongation gauge length varies from standard 2”

2.3 Test Procedure

As mentioned in Section 2.1, two hydraulic actuators working in parallel were used to apply cyclic axial displacements to the sliding beam while the opposite end remained fixed in place. Previous Research (Lehman et al. 2022) included test series that were subjected to displacement protocols that mimicked near-fault and chevron loading conditions in addition to a symmetric-based loading protocol. For the same brace, minimal variance in axial deformation range was seen between loading protocols. All braces in this research were subjected to a symmetric cyclic loading protocol that was developed based on previous research at the UW SRL and recommendations for testing components of steel structures (ATC, 1992, Krawinkler, 2009). Cycles started by pulling the brace into tension until the target displacement and then reversed into compression to the same magnitude of target displacement. Two full cycles were conducted for each target displacement. The first six target displacements were small steps to observe the elastic behavior of the brace, initial global buckling, and yielding. The small steps increased until 0.75” after which target displacement steps increased to 0.5” every change in target displacement until brace failure.

3. Round HSS Results and Discussion

In this section, the test results from the twenty-one specimens will be reviewed to assess the impact of local and global slenderness on brace deformation capacity. Two brace tests are reviewed in detail as examples.

3.1 Comparison between 6.625x3/16 and 6.625x3/8 brace response

A brace with a larger diameter-to-thickness ratio (6.625x3/16: D/t = 38.1, L_c/r = 96.3) and smaller diameter-to-thickness ratio (6.625x3/8: D/t = 19.0, L_c/r = 98.9) are compared below. Note the local slenderness of the 6.625x3/8 meets AISC 341-22 highly ductile requirements and the 6.625x3/16 does not meet the highly or moderate ductile limit. The maximum out-of-plane displacement exhibited by both braces is shown in Figure 4. This damage state occurred at peak compressive deformation. The brace with a smaller D/t achieved larger out-of-plane deformation at its peak compressive cycle before fracture. Figure 5 compares the cupping region at peak compressive cycles for both specimens. The magnitude of the depth of cupping is comparable, but the cupping deformation is more concentrated in the brace with higher D/t. The initiation of cupping deformation results in large strain concentrations in the middle of the local cupping region. The smaller the area, the larger the strains. The large strains impose the onset of striations and tearing in the subsequent tension cycle at the outer edges of the previously compression region. Fracture occurs almost immediately after tearing.

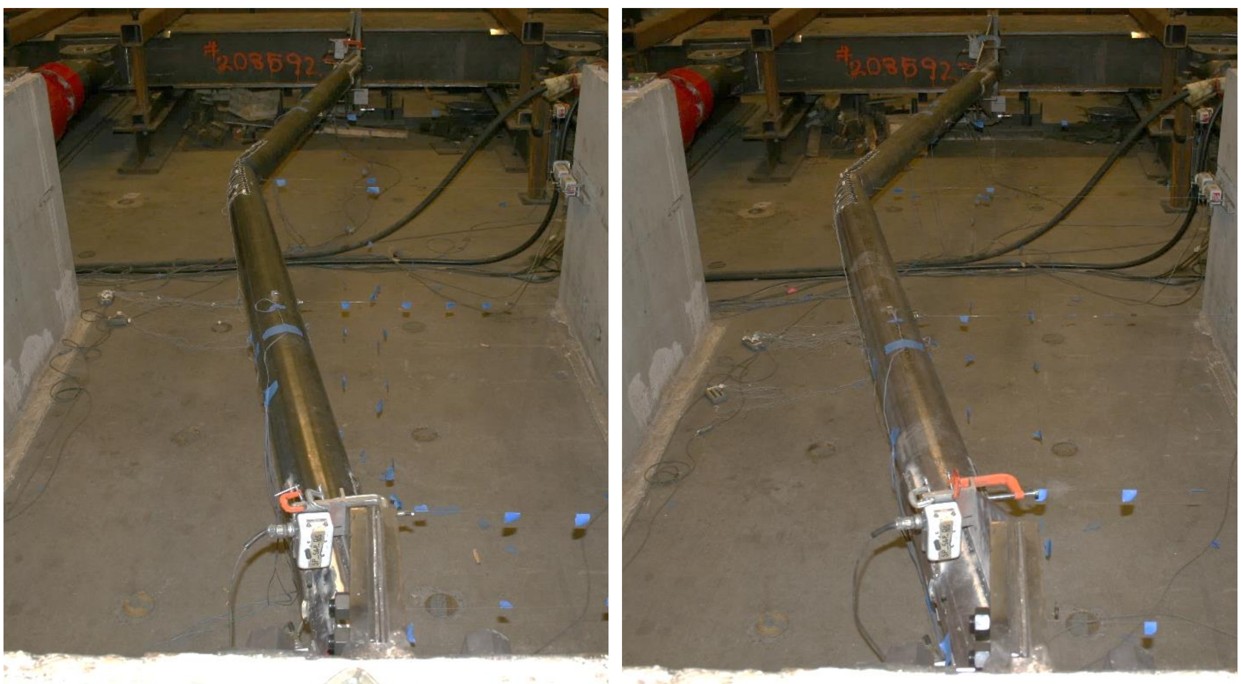

(a) (b)

Figure 4: Maximum brace out-of-plane displacement - 6.625x3/16 (a) and 6.625x3/8 (b)

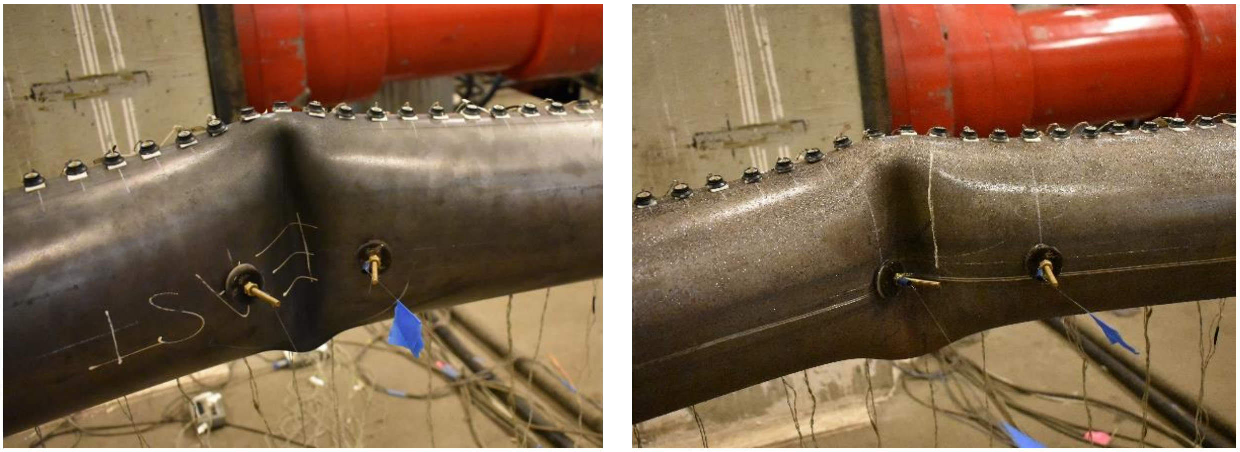

(a) (b)

Figure 5: Maximum cupping deformation at brace midspan – 6.625x3/16 (a) and 6.625x3/8 (b)

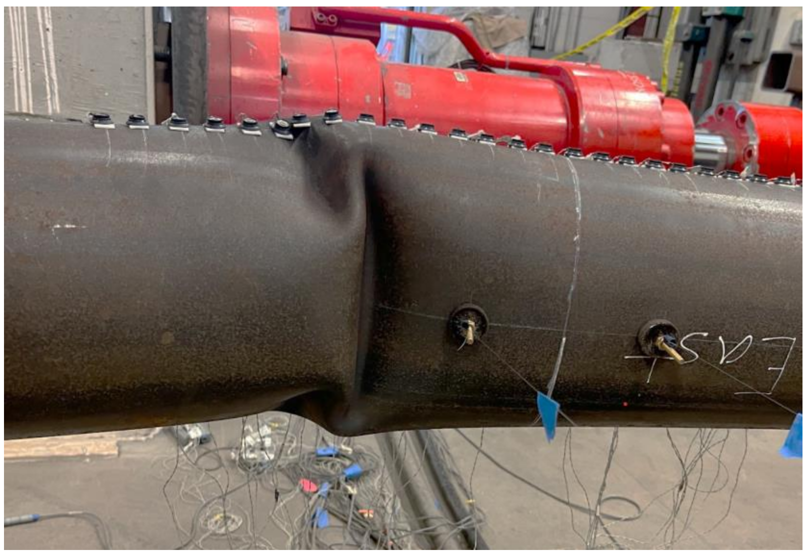

Figure 6: Local cupping region at brace midspan during peak compressive cycle - 8.625x3/16 S specimen

In some cases, the concentration of strains caused cupping around multiple locations as seen above in Figure 6. The larger main node of cupping is the first sign of visible local deformations, and the smaller nodes of cupping form in subsequent compression cycles. The local and global slenderness of this brace is 49.6 and 43.4 respectively. The combination of a very high diameter-to-thickness ratio and small global slenderness causes very large deformations at the locally deformed region. This type of local deformation is seen in other specimens with very large diameter-to-thickness ratios.

The normalized brace axial force-displacement hysteresis curves for the 6.625x3/16 and 6.625x3/8 specimens are shown in Figure 7 and Figure 8. The brace axial force is normalized by measured yield force utilizing yield strength, F_y from material testing (see Table 3). Axial deformation is normalized by the end-to-end brace length of the specimen. Damage states were identified for each test as the onset of global buckling, local cupping, striations and tearing, and brace fracture. Both braces reached brace yielding but came short of the expected peak compressive load. Their peak out-of-plane and in-plane displacement occurred at different cycles in the load history. For both braces, striations and tearing appeared in the tension cycle before fracture. The brace with a smaller local slenderness experienced more cycles before fracture than the brace with a larger local slenderness. While the number of cycles till fracture is greater in the brace with a smaller *D/t* ratio, the behavior post-initiation of cupping is the same. When cupping is first visible (damage state B-3C), fracture occurs two-and-a-half cycles later. Braces with smaller *D/t* ratios delay the onset of cupping allowing for larger axial deformation before fracture. This is why local slenderness is a critical variable in improving the deformability of brace systems.

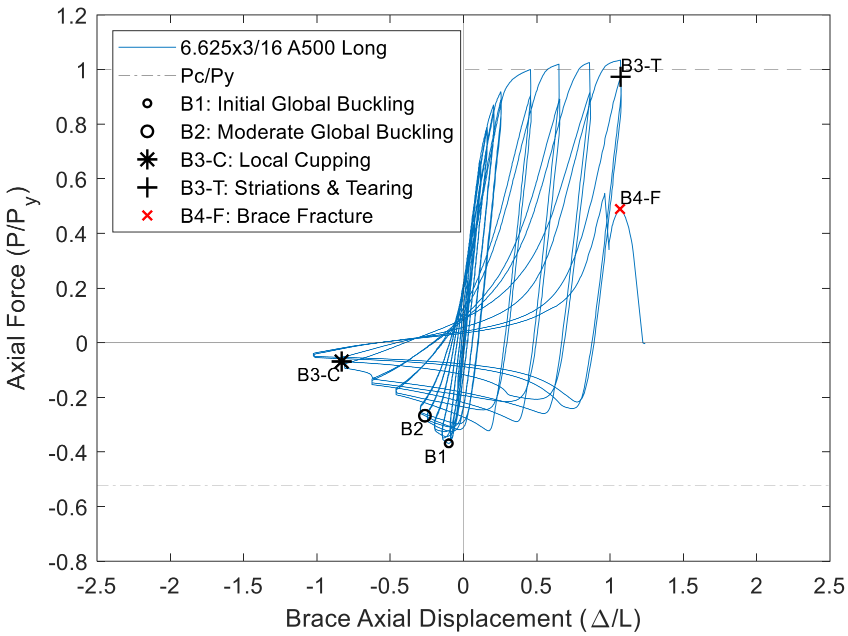

Figure 7: Force Displacement Response, 6.625x3/16

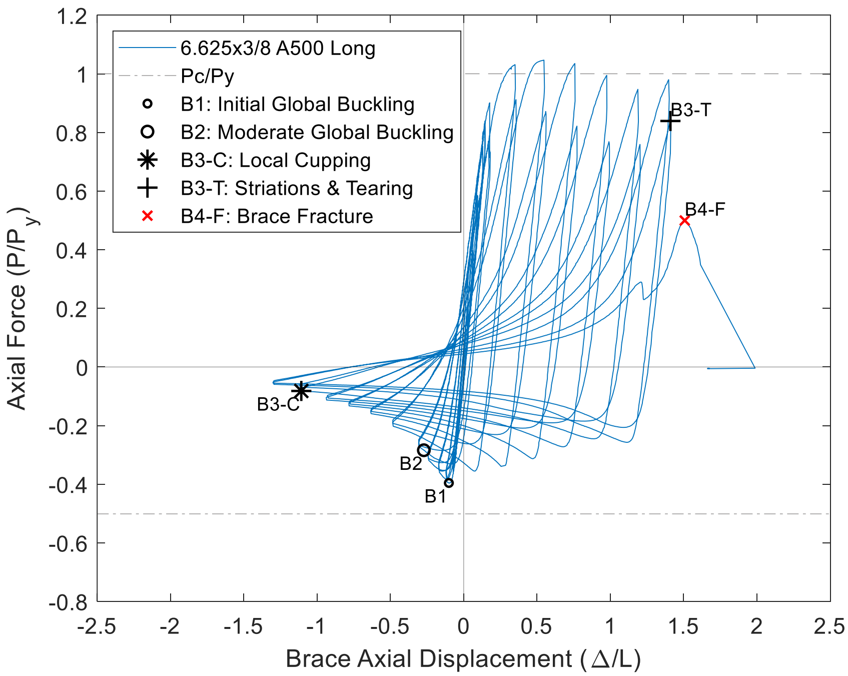

Figure 8: Force Displacement Response, 6.625x3/8

3.2 Summary of Test Results

The key results from testing are summarized in Table 4, including the normalized tensile deformation, normalized compressive deformation, and normalized deformation range at brace fracture. The deformation range is taken as the sum of tensile and compressive response. Brace local and global slenderness are noted to compare the effects of these properties on brace deformation capacity. Braces were expected to globally buckle towards the east side of the test setup due to the imposed connection eccentricity. Three out of the twenty-one braces did not buckle in the predicted direction and the effects of such may be reflected in the brace axial deformation range capacity.

Table 4: Summary of Test Results

Specimen	Geometric Properties		Normalized Axial Deformation (%)		
	D/t	L_c/r	def. ten	def. comp	def. range
6x3/16 S	34.5	89.1	1.22	1.12	2.34
6x3/16	34.5	106.6	1.30	1.14	2.45
6x1/4 S[1]	25.8	90.0	1.31	1.20	2.51
6x1/4[1]	25.8	107.6	1.63	1.45	3.08
6.625x3/16	38.1	96.3	1.07	1.02	2.09
6.625x1/4 S	28.4	81.2	1.38	1.40	2.79
6.625x1/4[1]	28.4	97.1	1.43	1.11	2.54
6.625x3/8 S	19.0	82.7	1.71	1.73	3.45
6.625x3/8	19.0	98.9	1.51	1.30	2.81
6.625x1/2 S	14.2	84.2	2.16	2.22	4.37
6.625x1/2	14.2	100.7	2.13	1.69	3.82
8.625x3/16 S	49.6	61.4	0.94	0.75	1.69
8.625x3/16	49.6	73.4	0.70	0.66	1.36
8.625x1/4 S	37.0	61.8	0.94	0.99	1.94
8.625x1/4	37.0	73.9	0.82	0.89	1.72
8.625x3/8 S	24.7	62.6	1.02	1.11	2.13
8.625x3/8	24.7	74.9	1.07	1.11	2.18
10.750x1/4 S	46.1	49.3	0.79	0.80	1.59
10.750x1/4	46.1	59.0	0.70	0.67	1.38
10.750x0.365 S	31.7	49.9	1.13	1.09	2.22
10.750x0.365	31.7	59.6	0.96	0.90	1.86

1. Braces that did not globally buckle in the predicted direction

The variation of normalized axial displacement range versus measured diameter-to-thickness (a) and brace global slenderness (b) is plotted in Figure 9. A power function is shown that fits the experimental data in plot (a) with an R-squared value of 0.862, which shows a good correlation between the Diameter-to-thickness and brace axial deformation capacity. The trend of data shows that as the brace diameter-to-thickness ratio increases, the brace axial deformation range decreases. This trend is consistent with data from previous research. The figure indicates that the effect of local slenderness on axial deformation range is exponential. At a higher value of local slenderness, a change in *D/t* causes a smaller effect on the deformation range than it does at a low value of local slenderness. The current AISC 341-22 highly, λ_{hd}, and moderately, λ_{md}, ductile limits are displayed in Figure 9 (a). As part of a coordinated research effort, Sen (2024) established target drift range capacities for SCBFs and OCBFs using non-linear multistory analysis. These deformation capacity targets are crucial for evaluating the current local slenderness limits. The target deformation capacity targets for SCBFs and OCBFs are plotted in terms of normalized axial displacement range.

Specimens that currently meet the highly ductile limit achieved a normalized brace axial deformation range of at least 2.8% and the axial deformation range target for SCBFs is 2.5%. The specimens that currently meet the SCBF requirement meet the SBCF target range in addition to 4 more specimens. Braces that currently meet the moderately ductile limit all reached a normalized axial deformation range greater than 2.0% and the axial deformation range target is 1.75%. Many other specimens with diameter-to-thickness ratios between 25-35 still achieved a 2.0% deformation range. All but four specimens that do not meet the current OCBF limit meet the target axial deformation range. The target for SCBFs and OCBFs heavily suggests that the deformation capacity of round HSS with local slenderness exceeding current limits is larger than target deformation values for moderate and highly ductile braces.

Figure 9 (b) shows the relationship between global slenderness and normalized brace axial displacement. The global slenderness of specimens ranged from 49.3 to 107.6. A linear function is fitted to experimental data in plot (b) with an R-squared value of 0.336. The trend of the data suggests that as brace global slenderness increases, brace axial deformation range increases. The figure indicates that the dependence of the axial deformation capacity to D/t is larger than L_c/r, but there is still a weak trend. A brace with a D/t = 25.8 (meets the moderately ductile limit), reached a normalized brace axial displacement range of 2.51%. A brace with a significantly larger diameter-to-thickness ratio, D/t = 34.5, achieved almost the same brace axial deformation range, 2.45% but also had a larger L_c/r. HSS shapes with the same cross-section size have relatively the same global slenderness but can have very different local slenderness depending on the wall thickness. Incorporating brace global slenderness, L_c/r, in the AISC 341-22 limits would more accurately represent HSS brace deformation capacity.

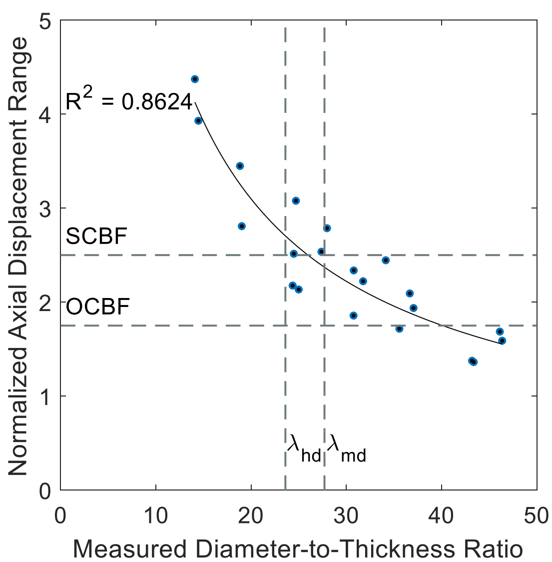

(a)

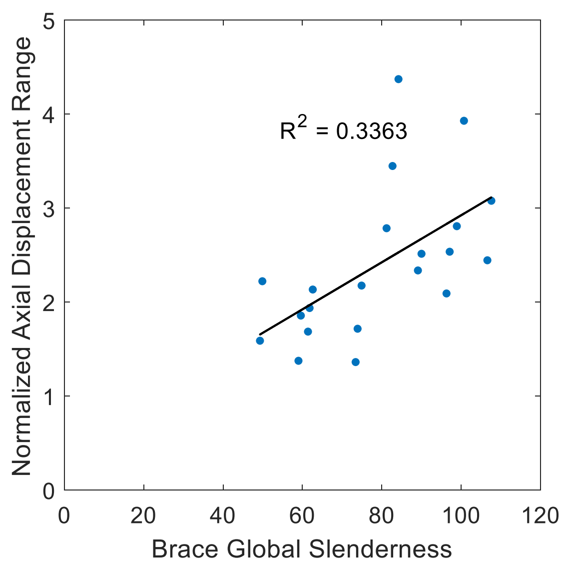

(b)

Figure 9: Effect of brace local slenderness (a) and global slenderness (b) on axial deformation range

4. Conclusions

A full-scale experimental program was undertaken to understand the relationship between local and global slenderness on HSS brace deformation capacity. Twenty-one brace specimens were subjected to a symmetric cyclic loading protocol until fracture. The tested specimens revealed the anticipated result that as the diameter-to-thickness ratio increases, brace axial deformation capacity decreases. A brace with smaller diameter-to-thickness delays the onset of cupping and limits the strain concentration in the deformed region. The data suggests that the deformation capacity of round HSS with local slenderness exceeding current limits is larger than target deformation values for moderate and highly ductile braces. While the trend was small, brace global slenderness, L_c/r, was also found to influence brace deformation behavior. As global slenderness increases, brace deformation capacity increases. A better fit of brace deformation capacity for the moderate and highly ductile limit should include both D/t and L_c/r and be formulated such that brace deformation capacity has a larger dependence on local slenderness than it does on global slenderness. Using composite sections such as concrete-filled HSS could further delay the onset of cupping and increase the compressive deformation capacity of the brace. Research on such should be explored to enhance the understanding of how composite HSS sections could positively affect braced frame system performance.

Acknowledgments

This research was possible thanks to the funding provided by the American Institute of Steel Construction (AISC) and the supply of material from Nucor Tubular Products and Searing Industries. A special thanks to UW SRL lab manager, Vince Chaijaroen, and all the undergrad research assistants who gave their time and energy to help with this project.

References

AISC (2024). "Seismic Provisions for Structural Steel Buildings." ANSI/AISC 341-24, American Institute of Steel Construction, Chicago, IL.

ASTM (2024). "Standard Test Methods and Definitions for Mechanical Testing of Steel Products." ASTM A370-24a, ASTM International, West Conshohocken, PA.

ATC (1992). "Guidelines for Cyclic Seismic Testing of Components of Steel Structures for Buildings." Report ATC-24, Applied Technology Council, Redwood City, CA.

Bergendahl, W, (2021). “Experimental Investigation to Compare the Cyclic Response of A500 and A1085 HSS Braces.” MS Thesis, University of Washington, Seattle.

Elchalakani, M., Zhao, X.-L., & Grzebieta, R. (2003). Tests of Cold-Formed Circular Tubular Braces under Cyclic Axial Loading. Journal of Structural Engineering, 129(4), 507–514.

Fell, B. V., Kanvinde, A. M., Deierlein, G. G., and Myers, A. T. (2009). "Experimental Investigation of Inelastic Cyclic Buckling and Fracture of Steel Braces." Journal of Structural Engineering, 135(1), 19-32.

Kaldestad, J, (2022). “Experimental Investigation into the Cyclic Response of A1085 HSS Braces” MS Thesis, University of Washington, Seattle.

Krawinkler, H. (2009). Loading Histories for Cyclic Tests in Support of Performance Assessment of Structural Components.

Sen, A. D., Ziccarelli, A., Berman, J. W., Roeder, C. W, Lehman, D. E., Jacinto, C. (2024). “Task Group Report on Seismic Local Buckling Limits – Braces Working Group” Task Group report, AISC, October, 2024.

Takeuchi, T., & Matsui, R. (2011). Cumulative Cyclic Deformation Capacity of Circular Tubular Braces under Local Buckling. Journal of Structural Engineering, 137(11), 1311–1318.